Electronic structure of one-dimensional copper oxide chains in LiCu$_2$O$_2$ from angle-resolved photoemission and optical spectroscopy

M. Papagno,[1,2] D. Pacilé,[1,2] G. Caimi,[3] H. Berger,[4] L. Degiorgi,[3] and M. Grioni[1]

[1]*Ecole Polytechnique Fédéderale de Lausanne, Institut de Physique des Nanostructures, CH-1015 Lausanne, Switzerland*
[2]*Istituto Nazionale di Fisica Nucleare (INFN), Dipartimento di Fisica, Universitá della Calabria, 87036 Arcavacata di Rende, Cosenza, Italy*
[3]*Laboratorium für Festkörperphysik, ETH Zürich, CH-8093 Zürich, Switzerland*
[4]*Ecole Polytechnique Fédéderale de Lausanne, Institut de Physique de la matière complexe, CH-1015 Lausanne, Switzerland*

Angle-resolved photoemission (ARPES) and optical measurements were performed on single crystal samples of LiCu$_2$O$_2$, an antiferromagnetic $S=1/2$ spin-chain compound. The ARPES spectra show several dispersive branches associated with hybrid copper-oxygen states. The occurrence of the valence band maximum halfway between the center and the edge of the Brillouin zone, and the complex spectral line shapes are not reproduced by the existing calculations of the electronic structure. We suggest that they can be interpreted within a one-dimensional scenario of strongly correlated antiferromagnetic insulators. The combination of ARPES and optics allows us to estimate the magnitude of the charge-transfer gap ($\Delta=1.95$ eV). Moreover, the temperature-dependent optical conductivity bears signatures of the three different magnetic phases of this material.

　　　　　　PACS number(s): 79.60.−i, 71.27.+a, 78.20.−e

I. INTRODUCTION

The electronic and magnetic properties of one-dimensional (1D) antiferromagnetic (AF) compounds based on copper-oxide chains or ladders[1–3] are subjects of strong ongoing interest. On the one hand, these systems are useful models to investigate the complex behavior of the two-dimensional high-T$_c$ superconductors. On the other hand, strongly correlated quasi-1D materials can be used to test the occurrence of exotic properties predicted by theory, beyond standard Fermi-liquid (FL) behavior.[4] The Tomonaga-Luttinger (TL) liquid concept sets the appropriate theoretical framework for metallic 1D correlated systems. In particular, the low-energy excitations in a 1D system are not the usual quasiparticles of Fermi-liquid theory, but consist of uncoupled collective spin and charge excitations. These spinons and holons can also be considered as new elementary particles, or new quantum states, resulting from a hole decay. The decoupled nature of these excitations leads to different velocities for spin and charge propagation, a phenomenon known as spin-charge separation.[5]

Angle-resolved photoemission spectroscopy (ARPES) can in principle address this quantum phenomenon, because it can directly measure the dispersion—and therefore the velocities—of both excitations. Hints of spin-charge separation have been reported in several ARPES studies of metallic quasi-1D materials and artificial epitaxial structures. In insulators, the possible observation of spin-charge separation was first claimed by Kim *et al.* for the 1D cuprate SrCuO$_2$,[6] where a good agreement between the ARPES results and the spectra predicted by a 1D *t-J* model led to the identification of spinon and holon branches. Further ARPES indications of anomalous spectral behavior have been subsequently reported in other insulating 1D compounds.[7,8]

Signatures[9] of exotic properties, deviating from the FL framework, have also been seen in the optical spectra of 1D correlated systems, like the well-known linear chain organic Bechgaard salts.[10] A dimensionality driven insulator-to-metal transition was discovered in these salts, by increasing the interchain coupling $t_\perp$. A strict 1D Tomonaga-Luttinger liquid is unstable towards Umklapp scattering processes, so that a Mott insulator develops for $t_\perp=0$ with the opening of the charge correlation gap E$_g$. Indeed, optical data clearly identified the absorption due to E$_g$ in the (TMTTF) family of Bechgaard salts.[10] When $t_\perp$ is enhanced by chemical or hydrostatic pressure, there is a confinement-deconfinement crossover of the quasiparticles, leading to a doped Mott-semiconductor, characterized by a Drude term in the excitation spectrum, together with the pseudo charge correlation gap.[9] These latter features have been discovered in the (TMTSF) family of organic salts.[10]

In general, optical experiments are a powerful bulk sensitive spectroscopy, allowing us to address the complete excitation spectrum. Of particular relevance are those excitations, revealing the electronic interband transitions, as well as the low frequency absorption spectrum, shedding light on the lattice dynamics (phonon modes).

In this paper we address the electronic structure of the quasi-1D insulator LiCu$_2$O$_2$. The orthorhombic unit cell of this material ($a=5.73$ Å, $b=2.859$ Å, and $c=12.419$ Å)[11] contains an equal number of Cu$^+$ and Cu^{2+} ions. The magnetic Cu^{2+} ($S=1/2$) ions are located at the center of edge-sharing CuO$_4$ plaquettes which form infinite chains along the crystallographic *b*-axis.[12–14] These chains are connected by chains of Li ions to form double layers parallel to the *ab* plane, which are separated by magnetically inert Cu$^+$ planes. Pairs of staggered chains from adjacent double layers are also weakly connected along the *c*-axis via 90° Cu-O-Cu bonds in a triangular ladder configuration. Within each chain the Cu-O-Cu bonds are nearly orthogonal ($\theta=94°$) [Fig. 1(a)]. As a consequence, the nearest-neighbor (NN) Cu-Cu
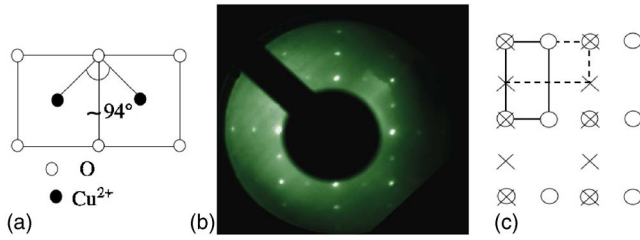
FIG. 1. (Color online) (a) Schematics of the edge-sharing CuO_4 units of $LiCu_2O_2$. The LEED pattern of the cleaved (001) surface (b) is the superposition of two rectangular ($a \sim 2b$) pattern rotated by 90° with respect to each other (c). Solid and dashed lines correspond to two different domains involving different Bragg peaks (crosses and circles).

interaction is weaker than the interaction between two next-nearest-neighbor (NNN) copper ions, and also weaker than the NN interaction in cuprates with corner-sharing plaquettes.[6,7] According to the Goodenough-Kanamori rule, the NN exchange interaction (J_1) is weakly ferromagnetic (FM), while the NNN exchange (J_2) is antiferromagnetic, leading to frustration. The system exhibits a spin singlet phase for $T > 23$ K,[13] a long-range ordered state with heli-magnetic structure at $T \sim 23$ K,[15,16] and a second low temperature transition into a collinear antiferromagnetic phase at $T \sim 9$ K.[13] We note that this latter transition was not found in the magnetic susceptibility data of Ref. 14. Furthermore, no anomaly was detected at 9 K in the neutron diffraction experiment.[16] It has been argued that it might arise due to an impurity phase, most likely Li_2CuO_2, which is known to undergo an AF transition at about 9 K.[17]

Whereas the magnetic properties of $LiCu_2O_2$ have been largely investigated, much less is known of its electronic states. Information on the density of states (DOS) and on the strength of correlations is available from valence band and core level x-ray photoemission (XPS) measurements on scraped polycrystalline samples.[12] XPS, as well as optics and electron energy loss (EELS) measurements have been performed on the related compound Li_2CuO_2.[18] So far, the detailed band structure of $LiCu_2O_2$ remains unexplored.

Here we present combined ARPES and optical results on single crystal specimens which considerably extend our knowledge of the electronic structure of this compound. Namely, our data yield a direct estimate ($\Delta = 1.95$ eV) of the charge-transfer (CT) gap and show signatures of the three different magnetic phases in the temperature dependence of the optical spectral weight. From ARPES we find that the top of the valence band occurs halfway between Γ and the boundary of the Brillouin zone (BZ), in contrast with existing band structure calculations.[15] This observation, and the complex spectral line shape, are consistent with a 1D scenario of strongly correlated electrons.

II. EXPERIMENTAL

Large specimens ($4 \times 4 \times 2$ mm³) $LiCu_2O_2$ single crystals were grown by heating in air above 1100 K a mixture with the proper stoichiometric ratio of Li_2CO_3 and CuO, as de-

scribed in Ref. 12. X-ray diffraction measurements confirmed the absence of parasitic phases, and the known tendency of this material to exhibit 90° twinning within the *ab* plane. The samples were post-cleaved at room-temperature (RT ~ 300 K) at a base pressure of 1×10^{-10} mbar, to expose mirror like (001) surfaces. We utilized low-energy electron diffraction (LEED) to verify the sample orientation and surface quality. The LEED pattern of Fig. 1(b) is typical of a cleaved (001) surface. It can be interpreted as the superposition of two orthogonal ($a \sim 2b$) rectangular patterns [Fig. 1(c)].

For ARPES we used 21.2 eV (He I) and 40.8 eV (He II) photons from a monochromatized Gammadata He discharge lamp, and a SCIENTA 300 electrostatic hemispherical analyzer with energy and momentum resolution $\Delta E = 10$ meV and $\Delta k \pm 0.02$ Å^{-1}, respectively. The Fermi level position was determined from the metallic cutoff of a polycrystalline Ag film at $T = 30$ K. ARPES data were obtained by rotating the sample around the *a*-axis, and collecting the photoelectrons within the *b*-*c* mirror plane. The x-ray photoelectron spectra were measured using monochromatic Al $K\alpha$ radiation (1486.6 eV). The energy resolution determined from the Fermi level of a polycrystalline Ag film at $T = 30$ K was 0.3 eV. Measurements on several cleaves from various samples yielded reproducible results, namely for the dispersion of the spectral features. The background intensity varied with cleave quality, and generally increased with measurement time. All spectra reported here are from fresh surfaces measured within 6 hours of the preparation.

The reflectivity $R(\omega)$ was measured from the far-infrared (FIR) up to the ultraviolet (UV) with light linearly polarized either along the *a*-axis or the chain *b* direction. The temperature was varied from 2 up to 200 K and at selected temperatures the magnetic field dependence was investigated. The absorption spectrum represented by the real part $\sigma_1(\omega)$ of the optical conductivity is obtained through a Kramers-Kronig (KK) transformation of $R(\omega)$. Since $LiCu_2O_2$ is an insulator at all temperatures, $R(\omega)$ was extrapolated with the constant value $R(\omega = 30$ cm$^{-1})$ for $\omega \to 0$. Above the highest measurable frequency, $R(\omega)$ was extended into the electronic continuum with standard extrapolations $R(\omega) \approx \omega^{-s}$ ($2 < s < 4$). Details pertaining to the experiment can be found in Refs. 19 and 20.

III. RESULTS AND DISCUSSION

A. ARPES measurements

The XPS valence band and Cu $2p$ core level results, shown in Figs. 2(a) and 2(b), are in excellent agreement with the literature, but the valence band line shape is somewhat more structured than that of a polycrystalline sample.[12] The $2p$ spectrum exhibits strong spin-orbit split features at 933 eV ($j = 3/2$) and 953 eV ($j = 1/2$) with overlapping contributions from the Cu$^+$ and Cu^{2+} sites. The ~ 10 eV satellites correspond to $2p^5 3d^9$ final states, and are typical signatures of Cu^{2+}. At this photon energy the ratio of cross sections $\sigma(Cu3d):\sigma(O2p)$ is ~ 50,[21] and the valence band spectrum essentially reflects the Cu character in the valence states. A
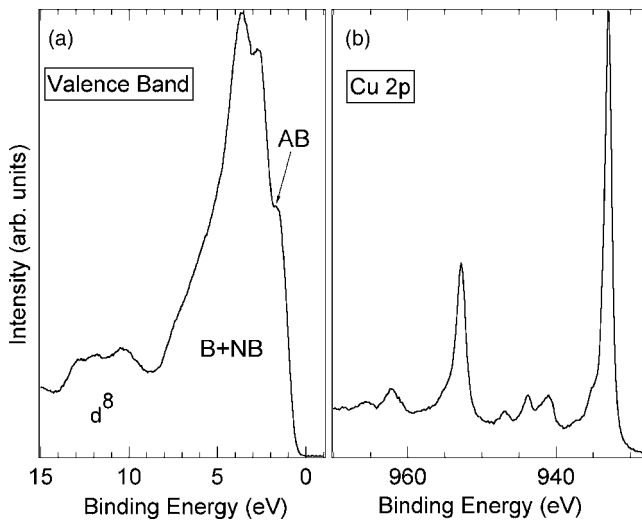
FIG. 2. (a) Al $K\alpha$ XPS valence band and (b) Cu $2p$ spectra of LiCu$_2$O$_2$. B and NB stand for bonding and nonbonding states, respectively, AB for antibonding states and d^8 for d^8 (Cu^{2+}) final state multiplet.

comparison with the XPS spectra of CuO and Cu$_2$O[22] shows that the signal from within $\sim$6 eV of E$_F$ is due to $3d^9\underline{L}$ $+3d^{10}\underline{L}^2$ (from Cu^{2+}) and $3d^9+3d^{10}\underline{L}$ (from Cu$^+$) final states, where $\underline{L}$ stands for a hole in the oxygen $2p$ band. In particular, the topmost feature at $\sim$1 eV has been attributed to $3d^9\underline{L}$ (Cu^{2+}) in Ref. 12. The deeper satellite at 10–12 eV is the d^8 (Cu^{2+}) final state multiplet, and its energy separation from the main feature is of the order (U$_{dd}-\Delta$), where U$_{dd}$ is the on-site Coulomb repulsion and Δ the charge-transfer energy. Therefore LiCu$_2$O$_2$, like most of the late $3d$ transition metal oxides, is a charge-transfer insulator (U$_{dd}>\Delta$) in the Zaanen-Sawatzky-Allen scheme of transition metal compounds.[23] Its electron removal ($E<0$) and electron addition ($E>0$) spectra can be schematically drawn as in Fig. 3. The first ionization state is the $3d^9\underline{L}$ Zhang-Rice local singlet (ZRS)[24] formed by an antibonding combination of Cu $3d$ and O $2p$ hole states on the same plaquette, which plays a major role in the high-T$_c$ cuprates. The ZRS is split off from a hybrid band of nonbonding (NB) O $2p$ and bonding (B) Cu-O states, while the deepest structure is the lower Hubbard band (LHB) of Cu d^8 character. The only relevant electron addition state is the upper Hubbard band (UHB) of
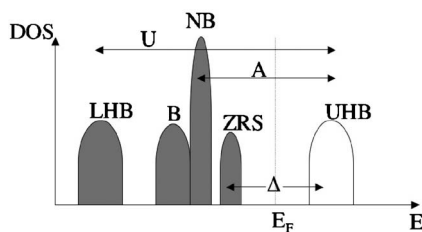

FIG. 3. Sketch of the density of states for the charge-transfer insulator. LHB stands for lower Hubbard band, ZRS for Zhang-Rice singlet state and UHB for upper Hubbard band. A is the transition between NB and UHB states. The optical (U) and the CT (Δ) gap are also shown.
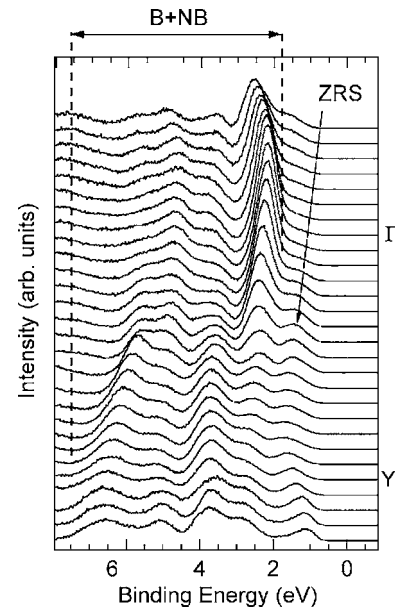

FIG. 4. Set of EDCs along the Y-Γ-Y direction obtained at RT with a photon energy hν=21.2 eV. The NB, B, and ZRS states are also shown.

Cu d^{10} character which defines, together with the ZRS, the charge transfer gap.

The XPS valence band spectrum is in qualitative agreement with the scheme of Fig. 3. The energy dispersion, namely of the ZRS, can be determined by ARPES. Figure 4 shows a set of energy distribution curves (EDCs) measured at RT and hν=21.2 eV, probing the band structure along the ΓY chain direction in the BZ. Several dispersive features can be identified within the broad B-NB manifold, including a prominent narrow ($\sim$0.5 eV) band around Γ, the center of the BZ, with a maximum at $\sim$2.1 eV. The ZRS band is the weaker structure which disperses around $\sim$1 eV, with maxima at 0.5ΓY and 1.5ΓY, and a minimum at the zone boundary Y. Its intensity is very low around Γ, i.e., at normal emission. This is due to the odd parity of the Cu $3d_{xy}$ orbital with respect to the b-c mirror plane, combined with the (partially) linearly polarized photons and the collection geometry, which selects even initial states, and causes a suppression of the photoemission intensity around Γ. The intensity increases with increasing emission angle, namely beyond Y into the second BZ. He II data (not shown) exhibit the same dispersion, but a larger intensity of the ZRS relative to the O $2p$ bands, as expected from cross section considerations for hybrid Cu d states.[21]

The dispersion and line shape of the ZRS band in the 2nd BZ are illustrated in Fig. 5. The He I ARPES spectra of Fig. 5(a) show a peak dispersing upward from 1.7 eV at Y, to $\sim$0.95 eV at 1.5ΓY. Beyond this point, the peak disperses back and broadens. A careful analysis of the spectral line shape suggests two separate underlying features, indicated by different symbols in the figure, which disperse with different velocities towards Γ', the center of the 2nd BZ. The overall dispersion of the prominent deeper peak (asterisk) mirrors the $Y\rightarrow1.5\Gamma Y$ dispersion. The shallower and weaker peak (full circle) exhibits a much reduced overall dispersion
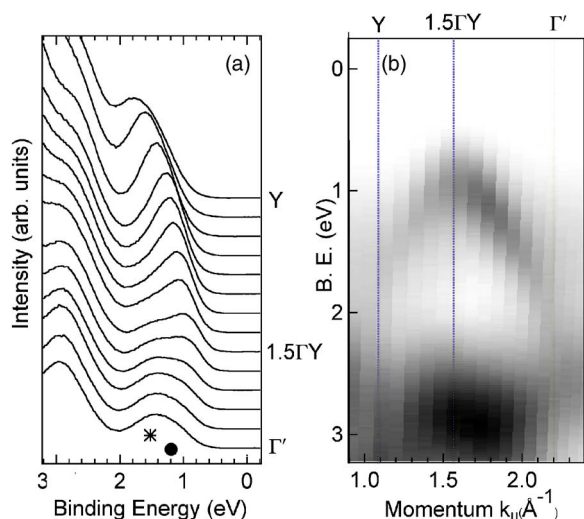
FIG. 5. (Color online) (a) EDCs obtained at RT with He-I line recorded in the second BZ. Two distinct features, indicated by an asterisk and a full circle, are seen to disperse with different velocities toward Γ'. (b) Intensity plot of the He-II data. A clear asymmetry between Γ' to $1.5\Gamma Y$ and $1.5\Gamma Y$ to Y is visible.

of $\sim$50–60 meV. Measurements along the transverse a-axis (not shown) yielded essentially identical results, reflecting the twinned nature of the sample.

The broader dispersion can be directly appreciated from the He II ARPES intensity map of Fig. 5(b). The maximum at $1.5\Gamma Y$ is again evident. Interestingly, unlike the 21.2 eV results of Fig. 5(a), at this photon energy the spectral weight distribution is dominated by the deeper peak. Moreover, the ARPES intensity is stronger for wave vector between $1.5\Gamma Y$ and Γ'. The weak shallow shoulder can only be identified by a careful analysis of the broad spectral line shape. In this analysis, after subtraction of an exponential inelastic background, we have looked for the best fit to the experimental spectra with the superposition of two Gaussian peaks. The ARPES results are summarized in Fig. 6 which illustrates the estimated dispersion of the ZRS and of the topmost O $2p$ band. The error bars represent the estimated uncertainties in the peak positions as determined by this phenomenological analysis.

We are not aware of first principle band structure calculations for LiCu$_2$O$_2$ taking proper account of electronic correlations, to be contrasted with the ARPES results. The LDA +U calculation of Zatsepin *et al.*[12] predicts LiCu$_2$O$_2$ to be a small gap (0.66 eV) insulator, but only the k-integrated density of states (DOS) has been reported. The k-resolved local density approximation (LDA) calculation of Gippius *et al.*[15] predicts a metallic ground state. If we use it nonetheless as a guideline for the band dispersion, we notice a qualitative discrepancy. The calculated bands exhibit a doubled periodicity in the chain direction, as a consequence of the dominant NNN interaction which effectively doubles the periodicity along the chain. Four tightly spaced bands are actually expected, due to the presence of two double-chains in the unit cell. However, all the calculated bands exhibit minima nearly halfway between Γ and the zone boundary, rather than a maximum.
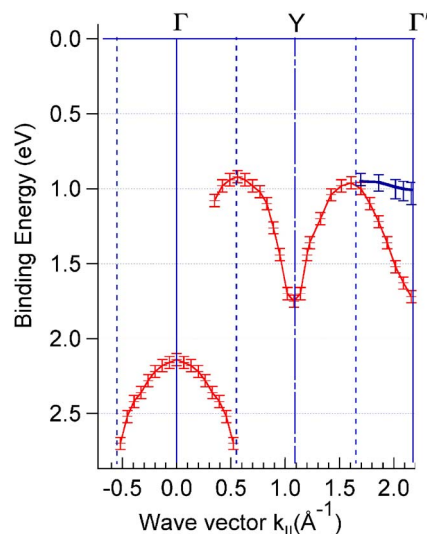

FIG. 6. (Color online) Dispersion extracted from data of Figs. 2 and 4. Between $1.5\Gamma Y$ and Γ' there are two bands assigned to the spinon and holon branches.

Our data suggest that strong correlations may be the actual origin of the observed double periodicity. The ZRS dispersion of Fig. 6 is qualitatively consistent with that of a half-filled band, as described, e.g., by an *effective* 1D Hubbard model. In this scenario strong electronic correlations open a gap at $k_F = \pi/(2b)$, and a shadow band disperses from the band maximum beyond that point. The ARPES results bear further resemblance with salient features of 1D models. The theoretical spectral function $A(k,\omega)$ of the 1D Hubbard or t-J models[25–27] consists of a narrow and shallow "spinon" band in the first half of the BZ, and a broader and deeper "holon" band, which exhibits a symmetric dispersion with respect to $k = 0.5\pi$.[6–8] t-J model calculations have shown that the motion of the charge is governed by the hopping term t, while the propagation of the spin excitation is governed by the exchange interaction J. The widths of the occupied spinon and holon bands are $\pi J/2$ and $2t$, respectively.[28] If we interpret the two features underlying the ARPES line shape of Fig. 5 along these lines, from the experimental dispersions we estimate $t \sim 0.37$ eV. For J we obtain $J \sim 35$ meV, but the uncertainty on this value is rather large due to the proportionally larger error bars on the spinon dispersion in Fig. 6. From $J = 4t^2/U_{dd}$, and for $U_{dd} \sim 8$ eV, which is typical for the cuprates, we would derive a somewhat larger $J = 68$ meV. This value is similar to those of other 1D correlated oxides,[8] and somewhat smaller, as expected, than the accepted J values in corner-sharing cuprates,[6,7] where the Cu-O-Cu interaction is larger. On the other hand, it is larger than the value obtained from a tight-binding fit of the LDA band.[15] It is also larger than J values commonly used to interpret the magnetic susceptibility[29] and the spin wave dispersion,[16] even if $J \sim 100$ meV apparently also yields a good fit to neutron diffraction data.[16] These discrepancies can be due to the uncertainties in the spinon dispersion. It could also point out the limitations of our analysis based on a minimal 1D nearest-neighbor t-J model, which is known to be too simplistic to fully describe the properties of this complex material.
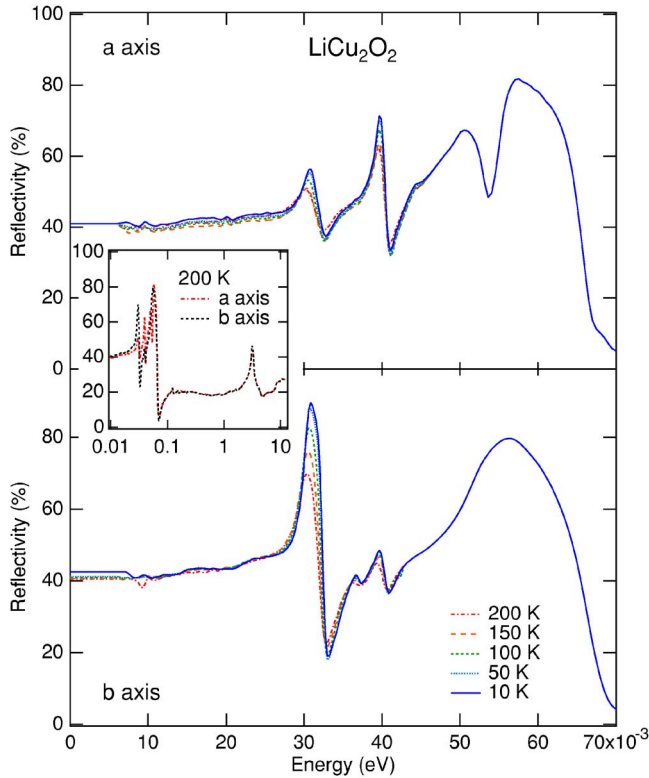
FIG. 7. (Color online) Temperature dependence of R(ω) at ω < 70 meV, for light polarized along the a- (upper panel) and b-axis (lower panel). Inset: R(ω) spectrum at 200 K up to the UV spectral range for both polarization directions.

The 1D t-J scenario predicts for the holon band a symmetric intensity distribution around $k = 0.5\pi$. We observe instead asymmetries of opposite sign at 21.2 and 40.8 eV. In the absence of a deeper analysis, we argue that this difference could be the result of ARPES matrix elements, reflecting the k-dependence of the Cu-O hybridization. Previous ARPES data, obtained at 21.2 eV with a similar sensitivity to the O 2p component of the band on SrCuO$_2$[6] and Sr$_2$CuO$_3$,[7] exhibit similar asymmetries. The model predicts also that the spinon and holon branches should have comparable intensities, while experimentally we observe a weaker spinon signal. Kobayashi *et al.*[30] have attributed a similar discrepancy in NaV$_2$O$_5$ to a finite temperature effect which leads to a spectral weight transfer from the spinon to the holon band. It has also been pointed out that extending the t-J model to include NNN interactions, which are of capital importance in LiCu$_2$O$_2$, similarly results in the suppression of the spinon branch.[6]

B. Optical measurements

We present in Fig. 7 the R(ω) data for both polarizations in the low frequency spectral range, where a temperature dependence is detected. For the sake of completeness, the inset of Fig. 7 displays the whole R(ω) spectra at 200 K. The real part $\sigma_1(\omega)$ of the optical conductivity is plotted in Fig. 8. The inset of Fig. 8 is a blow-up of the $\sigma_1(\omega)$ spectra at 200 K in the far infrared spectral range for both polarization
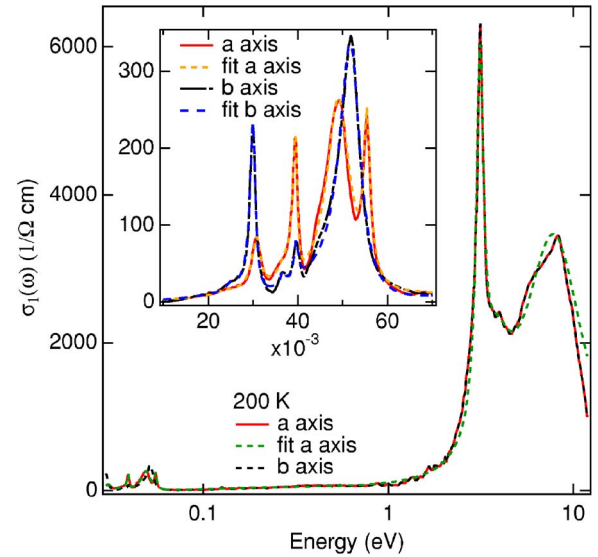

FIG. 8. (Color online) High frequency part of $\sigma_1(\omega)$ at 200 K for both polarizations. The Fano-Lorentz fit is also shown for light polarized along the a-axis. The inset is a blow up of the energy region pertinent for the phonon modes. The outstanding fit quality of the $\sigma_1(\omega)$ spectra is appreciable for both polarizations (see text).

directions, emphasizing the phonon modes of LiCu$_2$O$_2$. The R(ω) and $\sigma_1(\omega)$ optical spectra clearly demonstrate the insulating nature of LiCu$_2$O$_2$ at each temperature and for both polarizations, in agreement with the resistivity data.[31,32]

In Fig. 8 a huge absorption is observed at 3.1 eV (for both polarizations), followed by weaker interband absorptions at 3.8 and 7.8 eV. The huge resonance at 3.1 eV is related to an optical excitation typical of the edge sharing CuO$_4$ systems, and corresponds to an excitations from the O 2p nonbonding bands to the UHB (transition A in Fig. 3). We associate this prominent absorption peak to a transition from the narrow band at 2.1 eV in the ARPES spectra of Fig. 4. A similar feature has been identified in the absorption spectrum of Li$_2$CuO$_2$ by Mizuno *et al.*.[33] Their Hubbard model calculation also assigns a very small spectral weight to the ZRS → UHB transition across the charge-transfer gap (Δ), as a result of the reduced hopping probability of a hole along edge-sharing chains. This absorption feature cannot be directly identified at the leading edge of the main peak. Nevertheless, with the help of the ARPES data, which locate the top of the ZRS band at 0.95 eV and the NB band at 2.1 eV, we can determine the CT energy as $\Delta = 1.95$ eV (Fig. 3). Interestingly, this value is substantially larger than the LDA+U prediction.[12] We further assign the interband transitions observed in our spectra at 3.8 and 7.8 eV to transitions from the remaining nonbonding and bonding O 2p and Cu 3d states to the UHB.

We now move to the discussion of the phonon modes, which reveal information on the lattice dynamics and stress the relevance of interactions between lattice and electronic excitations. The electrodynamic response along the b-axis is characterized by two sharp phonons at 0.03 and 0.052 eV, and two weak modes at 0.036 and 0.039 eV. Along the a-axis, four major phonons are detected at 0.03, 0.04, 0.049 and 0.055 eV with an additional weak mode at 0.036 eV

(Figs. 7 and 8). The four phonons observed along the *b*-axis agree with the number of the B$_{2u}$ modes predicted by group theory.[34] On the other hand, along the *a*-axis, our measurement only detects five modes, less than the predicted nine B$_{3u}$. The energies of the modes along the *a*-axis are similar to those observed along the *b*-axis and such a similarity in the mode energies, as well as in their number, is due to twinning in our sample. Furthermore, other techniques reported similarities between the *a*- and *b*-axes. For example, the first x-ray experiment established for LiCu$_2$O$_2$ a D$_{4h}$ point group, where the rotation by $\pi/2$ along the *c*-axis is a symmetry of the system.[35] This is of course reflected in the uniformness of the electrodynamic response, particularly as far as the lattice dynamics is concerned.

In order to quantitatively analyze the electrodynamic response at different temperatures and polarizations, each $\sigma_1(\omega)$ curve has been fitted with the Fano's formula:[36,37]

$$\widetilde{\sigma}(\omega) = \sum_j i\sigma_{0j}\frac{(q_j+1)^2}{i+x_j(\omega)} \tag{1}$$

with $x_j(\omega) = \frac{\omega_{0j}^2 - \omega^2}{\Gamma_j \omega}$, where ω_{0j} is the resonance frequency, Γ_j is the width (i.e., damping) and $\sigma_{0j} = \omega_{pj}^2/\Gamma_j q_j^2$ with ω_{pj} as the oscillator strength and q_j as the so-called asymmetric factor of the *j*-mode. The asymmetric line shape of the phonon modes derives primarily from an interaction between the lattice vibrations and a continuum, usually given by an electronic background. The interaction with a magnetic continuum may also lead to a Fano line shape.[38]

It turns out that only the modes at 0.03 and 0.052 eV along the *b*-axis and the modes at 0.03, 0.04 and 0.049 eV along the *a*-axis are asymmetric. All other modes have a symmetric (Lorentzian) line shape (i.e., $q \to \infty$). The quality of fit at any temperature is astonishingly good, as demonstrated by the fit of $\sigma_1(\omega)$ at 200 K (Fig. 8). Furthermore, the same set of fit parameters used to account for the real part of the optical conductivity fits equally well the reflectivity curves. As seen in Fig. 7, the phonons of both polarizations show a weak temperature dependence, with fit parameters changing smoothly. Of particular interest is the temperature evolution of the phonon mode peaked at 0.03 eV (242 cm^{-1}) along the *b*-axis. This phonon gradually hardens by 1.2% as the temperature decreases from 200 down to 2 K. This hardening might be due to a freezing of the lattice motion. Furthermore, this is the only phonon showing a temperature dependent asymmetric line shape. Such an asymmetry is fitted with a negative *q* value in the Fano's approach.[36] The negative value of the asymmetry factor *q* indicates an interaction between the phonon mode and a temperature dependent electronic or magnetic continuum, extending over an energy interval below the resonance frequency of the mode. In the case of LiCu$_2$O$_2$, the continuum should be obtained by populating states with excitation energy $\Delta\epsilon/k_B \approx 72-73$ K, as suggested by the electron spin resonance and Raman spectroscopy.[13,39]

The temperature dependence of the interaction strength $1/q^2$ of the mode at 242 cm^{-1} is depicted in Fig. 9. The related asymmetry factor *q* is strongly enhanced with decreasing temperature, until it reaches a saturation around
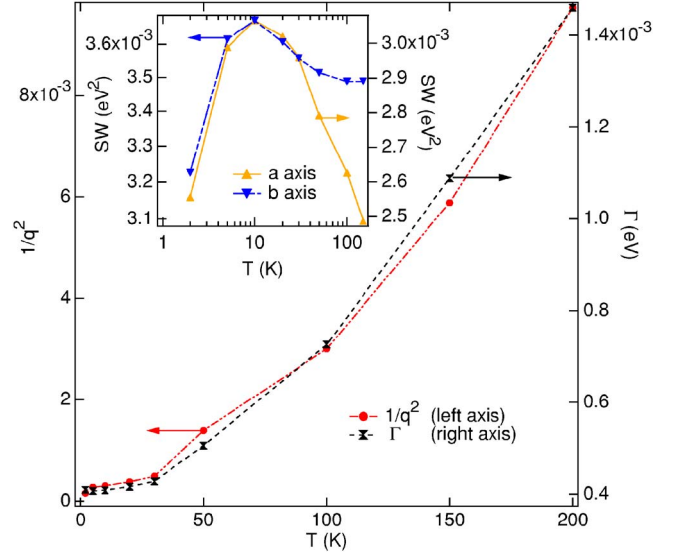

FIG. 9. (Color online) Scattering rate Γ and interaction strength $1/q^2$ of the phonon mode at 30 meV along the *b*-axis. The inset shows the temperature dependence of the spectral weight (SW) for both polarizations. Note the different *y*-scales for SW along *a*- and *b*-axis. The two *y*-scales have been shifted in such a way that the maximum of both SW around 10 K coincides.

30 K, below which an almost symmetric (Lorentzian) line shape develops. Simultaneously, this phonon mode, interacting with the continuum, gets narrow by lowering the temperature, as demonstrated by the decrease of its damping Γ at low *T* (Fig. 9). It is quite of interest that these two parameters show an analogous temperature dependence: the phonon's lifetime seems to be directly correlated with the increase of the phonon-continuum interaction $1/q^2$. The increase of $1/q^2$ with increasing temperature indicates that the interaction with the continuum is more important at high than at low temperatures. The continuum is indeed thermally populated at high *T*, allowing an interaction with the phonon mode at 242 cm^{-1}. On the other hand, at low *T* there are no excited states in the continuum and the interaction between continuum and phonon disappears (Fig. 9). The reduction of the scattering rate Γ at low *T* supports this picture. The phonon lifetime $\tau = 1/\Gamma$ is large below 30 K, where the continuum is indeed no longer populated.

Finally, we briefly address the temperature dependence of the spectral weight (SW), obtained by integrating $\sigma_1(\omega)$ from 0 up to 33 meV (i.e., a frequency just above the first phonon mode). The integration limit of about 33 meV defines the upper limit of the spectral range, within which a significant temperature dependence of SW has been found for both polarizations. The temperature dependence of SW is then plotted in the inset of Fig. 9 for both polarizations. One notes that SW has a broad peak centered at about 9 K and extending between 5 and 20 K, while below 5 K SW has a sudden drop. Above 20 K, there is a reduction of the SW by increasing the temperature along the *a*-axis, while along *b* the SW reduction is softer. Such a temperature dependence of SW gives evidence of the three different phases in LiCu$_2$O$_2$.[13] The pronounced SW reduction below 5 K might be connected with the antiferromagnetic phase transition detected at

9 K in several $LiCu_2O_2$ samples. Since this transition might be due to some Li_2CuO_2 inclusions, our data would then signal the presence of such impurity domains. However, we stress once again that our specimen does not apparently contain parasitic phases. It then remains to be seen, whether the transition at 9 K could be definitely assigned to an intrinsic phase of $LiCu_2O_2$. In fact, even recent neutron diffraction data[16] did not give evidence of such a transition at 9 K in the magnetic Bragg intensity. The broad peak in the SW extending up to 20 K reflects the long range ordered magnetic phase between 9 and 23 K, while once the temperature increases above 23 K and the system should enter in the phase associated with the gapped spin singlet state, $LiCu_2O_2$ reacts then with a decrease of SW.

IV. CONCLUSIONS

We performed angle-resolved photoemission and optical measurements on single crystal samples of $LiCu_2O_2$. Our ARPES data show dispersive electronic states associated to the B+NB states and to the Zhang-Rice local singlet. The ARPES results are not explained by LDA band structure, but can be interpreted in the framework of a strongly correlated 1D model. In $LiCu_2O_2$ this approach seems justified by structural considerations—the obvious chain structure—and also by the 1D nature of its magnetic properties. Combining ARPES and optical data we are able to evaluate the CT gap $\Delta \sim 2$ eV and the optical interband excitation between the NB and UHB states at 3.1 eV. Our optical data reveal a characteristic temperature dependence of the optical spectral weight in the far infrared range which reflects the transitions between the three different magnetic phases.

[1] A. Keren, L. P. Le, G. M. Luke, B. J. Sternlieb, W. D. Wu, Y. J. Uemura, S. Tajima, and S. Uchida, Phys. Rev. B **48**, 12926 (1993).

[2] M. Takano, Z. Hiroi, M. Azuma, and Y. Takeda, Jpn. J. Appl. Phys., Part 1 **7**, 3 (1992).

[3] E. Dagotto and T. M. Rice, Science **271**, 618 (1996).

[4] E. H. Lieb and F. Y. Wu, Phys. Rev. Lett. **20**, 1445 (1968).

[5] T. Giamarchi, *Quantum Physics in One Dimension* (Oxford Science Publications, New York, 2004).

[6] C. Kim, A. Y. Matsuura, Z.-X. Shen, N. Motoyama, H. Eisaki, S. Uchida, T. Tohyama, and S. Maekawa, Phys. Rev. Lett. **77**, 4054 (1996); C. Kim, Z.-X. Shen, N. Motoyama, H. Eisaki, S. Uchida, T. Tohyama, and S. Maekawa, Phys. Rev. B **56**, 15589 (1997).

[7] H. Fujisawa, T. Yokoya, T. Takahashi, S. Miyasaka, M. Kibune, and H. Takagi, Phys. Rev. B **59**, 7358 (1999); H. Fujisawa, T. Yokoya, T. Takahashi, S. Miyasaka, M. Kibune, and H. Takagi, Solid State Commun. **106**, 543 (1998).

[8] K. Kobayashi, T. Mizokawa, A. Fujimori, M. Isobe, and Y. Ueda, Phys. Rev. Lett. **80**, 3121 (1998).

[9] T. Giamarchi, Physica B **230-232**, 975 (1997).

[10] V. Vescoli, L. Degiorgi, W. Henderson, G. Grüner, K. P. Starkey, and L. K. Montgomery, Science **281**, 1181 (1998).

[11] R. Berger, P. Önnerud, and R. Tellgren, J. Alloys Compd. **184**, 315 (1992).

[12] D. A. Zatsepin, V. R. Galakhov, M. A. Korotin, V. V. Fedorenko, E. Z. Kurmaev, S. Bartkowski, M. Neumann, and R. Berger, Phys. Rev. B **57**, 4377 (1998).

[13] S. Zvyagin, G. Cao, Y. Xin, S. McCall, T. Caldwell, W. Moulton, L.-C. Brunel, A. Angerhofer, and J. E. Crow, Phys. Rev. B **66**, 064424 (2002).

[14] T. Masuda, A. Zheludev, A. Bush, M. Markina, and A. Vasiliev, Phys. Rev. Lett. **92**, 177201 (2004).

[15] A. A. Gippius, E. N. Morozova, A. S. Moskvin, A. V. Zalessky, A. A. Bush, M. Baenitz, H. Rosner, and S.-L. Drechsler, Phys.

Rev. B **70**, 020406(R) (2004).

[16] T. Masuda, A. Zheludev, B. Roessli, A. Bush, M. Markina, and A. Vasiliev, Phys. Rev. B **72**, 014405 (2005).

[17] E. M. L. Chung, G. J. McIntyre, D. McK. Paul, G. Balakrishnan, and M. R. Lees, Phys. Rev. B **68**, 144410 (2003).

[18] S. Atzkern, M. Knupfer, M. S. Golden, C. Waidacher, J. Richter, K. W. Becker, N. Motoyama, H. Eisaki, S. Uchida, and J. Fink, Phys. Rev. B **62**, 7845 (2000).

[19] F. Wooten, *Optical Properties of Solids* (Academic Press, New York, 1972).

[20] M. Dressel and G. Grüner, *Electrodynamics of Solids* (Cambridge University Press, Cambridge, 2002).

[21] J.-J. Yeh, *Atomic Calculation of Photoionization Cross-Sections and Asymmetry Parameters* (Gordon and Breach Science, Langhorne, 1993).

[22] J. Ghijsen, L. H. Tjeng, J. van Elp, H. Eskes, J. Westerink, G. A. Sawatzky, and M. T. Czyzyk, Phys. Rev. B **38**, 11322 (1988).

[23] J. Zaanen, G. A. Sawatzky, and J. W. Allen, Phys. Rev. Lett. **55**, 418 (1985).

[24] F. C. Zhang and T. M. Rice, Phys. Rev. B **37**, 3759 (1988).

[25] S. Sorella and A. Parola, J. Phys.: Condens. Matter **4**, 3589 (1992).

[26] K. Penc, K. Hallberg, F. Mila, and H. Shiba, Phys. Rev. Lett. **77**, 1390 (1996).

[27] J. Favand, S. Haass, K. Penc, F. Mila, and E. Dagotto, Phys. Rev. B **55**, R4859 (1997).

[28] P.-A. Bares, G. Blatter, and M. Ogata, Phys. Rev. B **44**, 130 (1991); M. Ogata, M. U. Luchini, S. Sorella, and F. F. Assaad, Phys. Rev. Lett. **66**, 2388 (1991).

[29] S.-L. Drechsler, J. Málek, J. Richter, A. S. Moskvin, A. A. Gippius, and H. Rosner, Phys. Rev. Lett. **94**, 039705 (2005).

[30] K. Kobayashi, T. Mizokawa, A. Fujimori, M. Isobe, Y. Ueda, T. Tohyama, and S. Maekawa, Phys. Rev. Lett. **82**, 803 (1999).

[31] A. A. Bush K. E. Kamentsev, and E. A. Tishchenko, Inorg. Mater. **40**, 44 (2004).

[32] A. A. Bush and K. E. Kamentsev, Phys. Solid State **46**, 445 (2004).

[33] Y. Mizuno, T. Tohyama, S. Maekawa, T. Osafune, N. Motoyama, H. Eisaki, and S. Uchida, Phys. Rev. B **57**, 5326 (1998).

[34] The space group Pnma (62) of $LiCu_2O_2$ corresponds to the D_{2h}^{16} point group. The total number of the expected modes after the correlation method turns out to be: $\Gamma^{Raman} = 10A_g(aa, bb, cc) + 5B_{1g}(ab) + 10B_{2g}(ac) + 5B_{3g}(bc)$ $\Gamma^{IR} = 9B_{1u}(E||c) + 4B_{2u}(E||b) + 9B_{3u}(E||a)$.

[35] S. J. Hibble, J. Köhler, and A. Simon, J. Solid State Chem. **88**, 534 (1990).

[36] U. Fano, Phys. Rev. **124**, 1866 (1961).

[37] G. Caimi, PhD. Thesis ETH Zürich (2005), unpublished.

[38] P. Lemmens, G. Güntherodt, and C. Gros, Phys. Rep. **375**, 1 (2003).

[39] K.-Y. Choi, S. Zvyagin, G. Cao, and P. Lemmens, Phys. Rev. B **69**, 104421 (2004).